

# **International Journal of Optomechatronics**



ISSN: 1559-9612 (Print) 1559-9620 (Online) Journal homepage: https://www.tandfonline.com/loi/uopt20

# Simultaneous multi-dimensional spatial frequency modulation imaging

Nathan Worts, John Czerski, Jason Jones, Jeffrey J. Field, Randy Bartels & Jeff Squier

**To cite this article:** Nathan Worts, John Czerski, Jason Jones, Jeffrey J. Field, Randy Bartels & Jeff Squier (2020) Simultaneous multi-dimensional spatial frequency modulation imaging, International Journal of Optomechatronics, 14:1, 1-17, DOI: <u>10.1080/15599612.2019.1694610</u>

To link to this article: <a href="https://doi.org/10.1080/15599612.2019.1694610">https://doi.org/10.1080/15599612.2019.1694610</a>

9	© 2019 The Author(s). Published with license by Taylor & Francis Group, LLC
	Published online: 06 Jan 2020.
	Submit your article to this journal 🗷
lill	Article views: 455
a`	View related articles 🗹
CrossMark	View Crossmark data 🗗







# Simultaneous multi-dimensional spatial frequency modulation imaging

Nathan Worts<sup>a</sup>, John Czerski<sup>a</sup>, Jason Jones<sup>b</sup>, Jeffrey J. Field<sup>c,d,e</sup>, Randy Bartels<sup>c,d</sup>, and Jeff Squiera

<sup>a</sup>Department of Physics, Colorado School of Mines, Golden, CO, USA; <sup>b</sup>Moog Inc, East Aurora, NY, USA; CDepartment of Electrical and Computer Engineering, Colorado State University, Fort Collins, CO, USA; <sup>d</sup>Department of Biochemistry and Molecular Biology, Colorado State University, Fort Collins, CO, USA; <sup>e</sup>Microscope Imaging Network Foundation Core Facility, Colorado State University, Fort Collins, CO, USA

#### **ABSTRACT**

One of the primary challenges in advanced manufacturing (AM) is the lack of efficient optical metrics for ensuring quality control over the manufacturing process. Many current imaging techniques have excessive data requirements and require computationally intensive post-processing to effectively characterize various AM environments. Spatial frequency modulated imaging (SPIFI) addresses many of these issues with the following benefits: it is compatible with long working distance optics, provides a large field-of-view, features single element detection, and can provide enhanced resolution. Here, we demonstrate SPIFI with enhanced resolution in multiple dimensions for the first time. This is achieved by incorporating multiple linear extended excitation sources oriented with axes at arbitrary angles with respect to each other. The system utilizes a single modulation mask enabling facile implementation within existing imaging systems such as those found in laser AM systems.

#### **KEYWORDS**

Spatial frequency modulation; imaging; single element detection; enhanced resolution; nonlinear imaging

#### 1. Introduction

SPatIal Frequency modulated Imaging, or SPIFI, is an exciting new paradigm for pushing the limits in quantitative imaging. [1,2] To our knowledge it is one of the first general methods for pushing the spatial resolution past traditional boundaries.<sup>[3]</sup> Notably, it does so under both linear and nonlinear excitation conditions, and with incoherent (e.g., linear or multiphoton excited fluorescence) and coherent (e.g., second and third harmonic generation) contrast mechanisms. SPIFI does this all the while incorporating extended excitation sources, such as a line (as opposed to a point focus) enabling a wide field-of-view<sup>[4]</sup> and optimal frame rates. Indeed, Diebold et al.<sup>[5]</sup> using radio frequency modulation methods and confocal linear fluorescence imaging, have achieved frame rates exceeding 4kHz. An especially attractive feature of SPIFI is that while an extended source is used for excitation, the signal light is collected through single element (point) detection such as with a photomultiplier tube or photodiode. By enabling one-dimensional imaging with point detection, SPIFI is robust in specimen environments where the excitation and/or signal light can be scattered. [6] SPIFI systems can also be configured to provide high resolution





CONTACT Jeff Squier 🔯 jsquier@mines.edu 🗈 Department of Physics, Colorado School of Mines, Golden, CO 80401-

1887, USA.

Color versions of one or more of the figures in the article can be found online at www.tandfonline.com/uopt.

depth information via the coherent holographic image reconstruction by phase transfer technique and the interferometric reflective geometry. [7–11]

Under the SPIFI paradigm, imaging systems can be transformed in significant new ways that include: (1) long working distance optics (e.g., >60 mm) can be used with unprecedented effectiveness by achieving a large field-of-view (e.g., >20 mm) with extended resolution independent of imaging modality, (2) single element detectors, often superior to their two-dimensional counterparts in terms of performance are employed, which in turn enables, (3) the imaging system to be effective when imaging into a scattering environment. In particular, in this article we show for the first time, multidimensional, enhanced resolution imaging achieved with a single SPIFI mask fabricated in-house. One of the strengths of the SPIFI method is that the enhanced resolution can be verified across imaging modalities. To date, for nonlinear imaging this has included using 100 nm fluorescent beads in two photon excitation fluorescence and using 200 nm BTO particles for second harmonic generation imaging to measure the point spread function and spatial cutoff frequency for these imaging modalities. [3] In linear imaging, standardized targets with varying, quantified spatial frequency content are imaged, and doubling of the pixel density is confirmed. [4]

# 1.1. Spatial frequency modulation imaging: breaking imaging limits

So how is SPIFI implemented? As we will show in this article, it is surprisingly straightforward, and existing systems can be readily adapted to exploit the SPIFI method. First, this imaging technique utilizes a cylindrical lens to focus the excitation beam to a line, effectively creating a light sheet. The light sheet is then incident on the SPIFI mask. The mask is fabricated in-house, as we will show in later sections, and is the heart of the SPIFI method. The mask is located at the focal plane of the cylindrical lens and is spun at a constant rate. The pattern on the mask is specifically designed such that it attenuates (modulates) the intensity of each resolvable pixel across the light sheet at a unique frequency which increases in a linear fashion across the mask. This enables single element detection. An alternative description is to note that as the mask spins, it transmits a spatial frequency that varies as a function of time. The mask is acting as a time-varying diffractive element: there is an emergence of light sheets (after the mask) which will be represented in this article by the three diffracted orders (-1, 0, +1). Finally, these diffracted orders are image relayed in a 4-f configuration to the focal plane of the imaging system with the desired magnification to achieve the highest resolution and desired field-of-view.

In the following subsections we create a step-by-step guide to understanding and implementing the SPIFI method. First, we examine the desirable characteristics the mask needs to modulate the light sheet in a manner compatible with single element detection. From these details, we can then extrapolate to the SPIFI mask design. Next, the optical platform incorporating the mask is discussed, and basic signal collection analysis is shown. Finally, we treat how this design leads to enhanced resolution, and present new results in two-dimensional enhanced resolution SPIFI imaging.

#### 1.1.1. Modulating the beam

Properly modulating the excitation or illuminating light sheet is key to forming an image with SPIFI. As a first step in creating a light sheet, the excitation laser beam is focused through a cylindrical lens and onto the mask. This produces our extended source: a line focus that, once transmitted through the mask, results in an amplitude modulation that varies in rate as a function of position across the line. The modulation by the mask can be modeled through a simple plane-wave analysis that treats the transmitted beams as a series of diffracted orders which can be

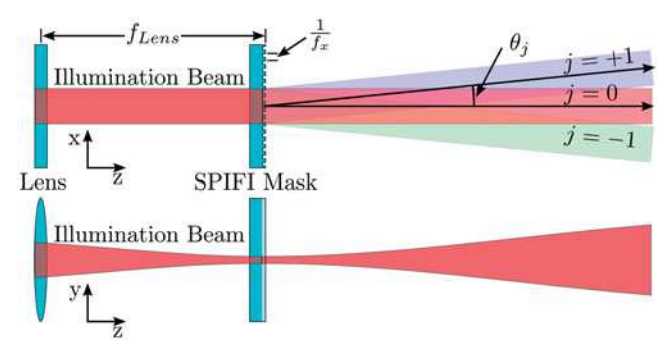


Figure 1. A cylindrical lens is used to create a light sheet that is focused and passed through a mask modeled as a diffraction grating. The upper figure is looking down on the system, the lower figure is the side view.

described with the grating equation,

$$\sin[\theta_j(t)] - \sin[\theta_{inc}] = jf_x(t)\lambda \tag{1}$$

where j is the order of the diffracted beam,  $\theta_j(t)$  is the angle of the diffracted beam,  $\theta_{inc}$  is the angle of the incident beam,  $f_x(t)$  is the time dependent spatial frequency of the modulation mask, and  $\lambda$  is the wavelength of the incident light. When the incident beam is normal to the surface of the mask, the equation can be simplified and solved to provide an expression for the angle of the diffracted beams.

$$\theta_i(t) = \arcsin[jf_x(t)\lambda] \tag{2}$$

Figure 1 shows the two transverse projections of the cylindrical lens, mask combination. The top view shows that the mask pattern modulates the beam across the x dimension resulting in the diffracted orders. As stated earlier, we limit our discussion and analysis to the three diffracted orders (-1, 0, +1). The lower view shows the beam focusing in the y dimension which is important for creating a sharp image of the mask pattern and maximizing the lateral resolution of the spatial frequency imprinted on the beam. These diffracted orders then pass through a simple 4-f system consisting of two spherical lenses as shown in Figure 2.

At the object plane, interference between the j=0 and  $j=\pm 1$  beams results in modulation at a spatial frequency corresponding to the angle between the beams. The electric field at the object can be approximately written as the sum of the plane waves corresponding to the diffracted orders,

$$\vec{E}_{tot}(\vec{r},t) = \sum_{j=-1}^{1} \vec{E}_{j}(\vec{r},t)$$
 (3)

where the electric field of the diffracted orders,  $\vec{E}_m$ , can be written,

$$\vec{E}_{j}(\vec{r},t) = a_{j}\vec{E}_{0}\cos\left[\vec{k}_{j}(t)\cdot\vec{r} - \omega_{optical}t\right]$$
(4)

where  $a_j$  is the amplitude coefficient of the diffracted order,  $\vec{k_j}(t)$  is the k-vector of the diffracted order, and  $\omega_{optical}$  the frequency of the light. The k-vector of the diffracted orders can be written in terms of the k-vector of the initial beam and the angle of diffraction,

$$\vec{k_i}(t) = k_0 \left( -\sin[\theta_i(t)] \hat{x} + \cos[\theta_i(t)] \hat{z} \right) \tag{5}$$

where  $k_0 = |\vec{k}_0|$  is the magnitude of the k-vector of the initial beam. Plugging in our solution for  $\theta_i(t)$  leads to,

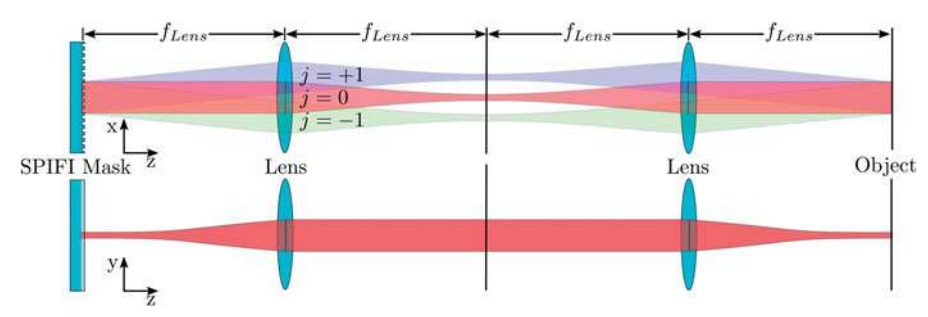


**Figure 2.** Orthogonal projections of illumination beam and its diffracted orders. The system is shown with lenses of equal focal length to simplify the figure. The diffracted orders are imaged onto the object.

$$\vec{k_j}(t) = k_0 \left( -f_x(t)j\lambda \ \hat{x} + \sqrt{1 - f_x^2(t)j^2\lambda^2} \ \hat{z} \right)$$
 (6)

The modulation of the electric field,  $\omega_{optical}$ , occurs many orders of magnitude faster (typical optical frequencies are on the order of  $10^{14}$  Hz) than the bandwidth of the detectors being used or the change in spatial frequency, so we can write the intensity of the beam,

$$I(x,t) = I_0 \left( a_0 + 2a_1 \cos \left[ 2\pi f_x(t)x \right] \right)^2 = I_0 a_0^2 + 4I_0 a_0 a_1 \cos \left[ 2\pi f_x(t)x \right] + 4I_0 a_1^2 \cos \left[ 2\pi \left( 2f_x(t) \right)x \right]$$
 (6)

where we have averaged out the time dependence of the electric field but kept the time dependence of the spatial frequency since it is effectively constant over the period  $T = 2\pi/\omega_{optical}$ . We also neglected terms with |j| > 1, and assumed  $a_{+1} = a_{-1}$ . Consequently, I(x,t) can be separated into a DC term and terms corresponding to the interference between the 0 and  $\pm 1$  order terms and interference between the +1 and -1 order terms. The standard resolution image is formed from the interference between the 0 and  $\pm 1$  terms,

$$I_1(x,t) = 4I_0 a_0 a_1 \cos[2\pi f_x(t)x]$$
 (8)

and the enhanced resolution image is formed from interference between the +1 and -1 terms. The intensity of this term,

$$I_2(x,t) = 4I_0 a_1^2 \cos\left[2\pi \left(2f_x(t)\right)x\right]$$
(9)

has twice the spatial frequency of the  $I_1(x,t)$  term. This process is visualized in Figure 3 which depicts the interaction between wavefronts of the various diffracted orders.

In a typical imaging system, the maximum spatial frequency passed by the imaging system is defined by the numerical aperture (NA),

$$f_{x,c} = \frac{NA}{\lambda} = \frac{n\sin[\alpha]}{\lambda} \tag{10}$$

where n is the index of refraction in the object region,  $\alpha$  is the semi-aperture angle, and  $\lambda$  is the wavelength of light. Figure 3 illustrates how interference between the j=0 and  $j=\pm 1$  terms result in the cutoff frequency,  $f_{x,c}$ , of a traditional imaging system, and how interference between the j=+1 and j=-1 rays results in the higher spatial frequency associated with the enhanced resolution SPIFI images. In fact, the enhanced resolution is equivalent to doubling the semi-aperture angle of the imaging system. This illustrates why SPIFI is such a powerful general method especially when long working distances are required. For a more detailed theoretical treatment see Higley et al. [12]

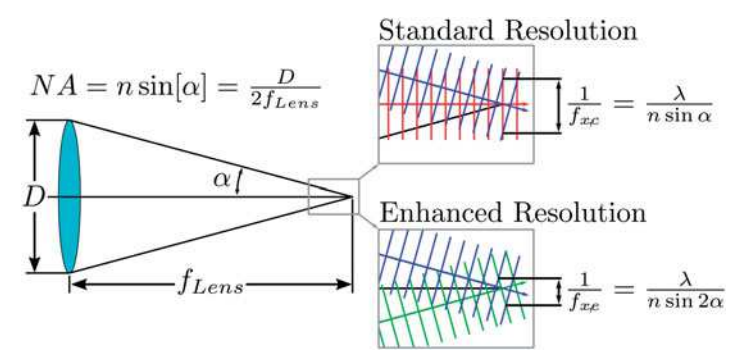


Figure 3. Diagram of interference between the diffracted orders. The standard resolution image is formed by interference between the j=0 and  $j=\pm 1$  orders. The enhanced resolution image is formed by interference between the j=+1 and  $j=\pm 1$ 

#### 1.1.2. SPIFI mask pattern

With a clear technique for producing a modulated beam on the sample, the next step is to choose a pattern for the SPIFI Mask that facilitates image reconstruction. The pattern we use is adapted from the Lovell reticle which has a linear relationship between modulation frequency and radial position. [13-15] The mask needs to contain all of the spatial frequencies necessary to take advantage of the NA of the imaging system, and the beam must sweep through these frequencies. The easiest way to accomplish this is by encoding the pattern into a radial geometry. This allows the pattern to be scanned through the beam by spinning the mask rather than altering the beam path.

The key to easily retrieving an image from the modulation pattern is the linear relationship between the x position in the beam and the frequency of modulation in time. This can be achieved with the equation,

$$m(x,t) = \frac{1}{2} + \frac{1}{2}\cos(2\pi\kappa xt)$$
 (11)

Where  $\kappa$  is a spatial and temporal frequency parameter,

$$\kappa = \frac{f_{x, max}}{T} \tag{12}$$

where  $f_{x,max}$  is the maximum spatial frequency on the mask and T is the period of oscillation. Figure 4(a) shows the 2D modulation pattern of Equation 11. As x increases, the temporal frequency of the modulation also increases. To induce a time varying spatial frequency phase that leads to a carrier frequency, the beam is offset from x = 0 to  $x = x_c$  which shifts the image location in the temporal frequency space (i.e., shifts the carrier frequency of the detected signal). This can be written in terms of a shifted coordinate,

$$m(x',t) = \frac{1}{2} + \frac{1}{2}\cos(\omega_c t + 2\pi f_x(t)x')$$
 (13)

where  $x' = x - x_c$  and  $\omega_c = 2\pi f_{x, max} x_c / T$ . We can convert this pattern to a radial representation with the line focus of the illumination beam along the radius,

$$m(\rho,\theta) = \frac{1}{2} + \frac{1}{2}\cos(f_c t + f_{x,max}\rho\theta)$$
(14)

where  $\rho$  is the position of the beam along the radius of the spinning mask and  $\theta$  is the time dependent angle of the mask. If the disk spins at a constant angular velocity  $\omega$  this can be written as,

$$m(\rho, t) = \frac{1}{2} + \frac{1}{2}\cos(\omega_c t + f_{x, max}\omega\rho t)$$
(15)

which is shown in Figure 4(b).

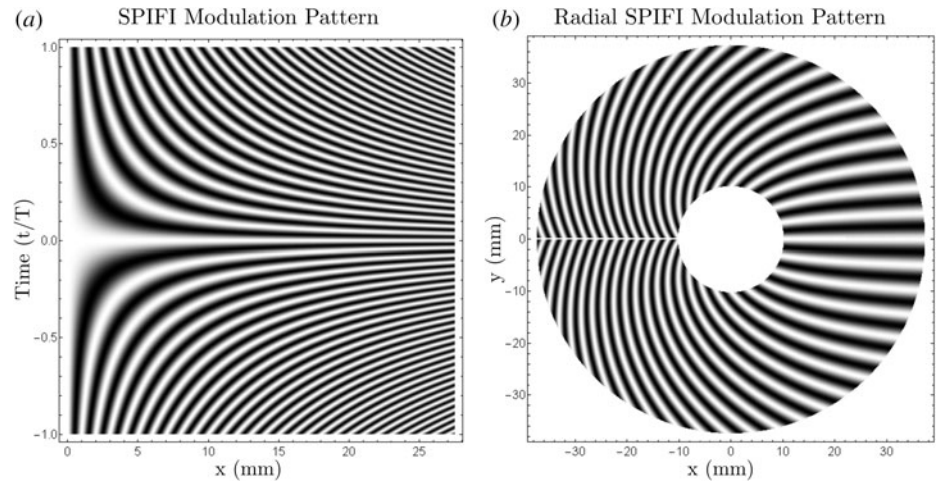


**Figure 4.** The SPIFI pattern for optimal image reconstruction. (a) The SPIFI pattern in time and spatial coordinates. Various positions along the x axis are modulated at different temporal frequencies, while maintaining a fixed spatial frequency at a given point in time. (b) The radial extension of (a). When spun at constant angular velocity, this pattern modulates the beam in a way that facilitates simple image reconstruction with a Fourier transform.

The full beam modulation system with the modulation mask is shown in Figure 5 which contains an Optics Studio ray-tracing of the illumination system.

# 1.1.3. Signal collection and analysis

As stated, the net excitation intensity given at the focal plane of the optical system is a sum of a DC term, interference between the  $j=\pm 1$  and j=0 terms, and interference between the j=+1 and j=-1 terms, as described in Equation 7. We can accommodate important effects such as vignetting as the light sheets are scanned across the entrance pupil of the imaging system by collecting the respective terms in 7 by a time dependent amplitude H(t), following the development of Field et al.<sup>[3]</sup> Recast in this manner, Equation 7 simplifies to:

$$I(x,t) = H_0(t) + H_1(t) \cos[2\pi f_x(t)x] + H_2(t) \cos[2\pi 2f_x(t)x]$$
(16)

A key feature of SPIFI is the enhanced resolution capability. Again, it is quite general as it will impact all contrast mechanisms and is already built into the system. There are no complex exposure conditions or special optics that need to be met to push the resolution limits. This becomes particularly clear with a simple analysis of the spatially integrated detected signal. The spatial integral corresponds to collecting the signal from the image plane onto a single element detector. The measured signal from our detector, S(t), is given by spatially integrating the signal light intensity,  $\beta(x,t)$ :

$$S(t) = \int_{-\infty}^{\infty} \beta(x, t) dx$$
 (17)

The signal light intensity is simply the product of the excitation intensity (16) with the optical response of the chosen contrast mechanism(s) C(x). In the most general case, the intensity can be driving the system in a linear or nonlinear fashion, hence the generalization of the functional form of the excitation intensity in the expression below.

$$\beta(x,t) = I^{\eta}(x,t)C(x) \tag{18}$$

Retrieval of the one-dimensional image from the signal S(t), is then quite straight-forward and is shown in Figure 6. A simple Fourier transform of the signal (in this case  $\eta=1$ ) yields two

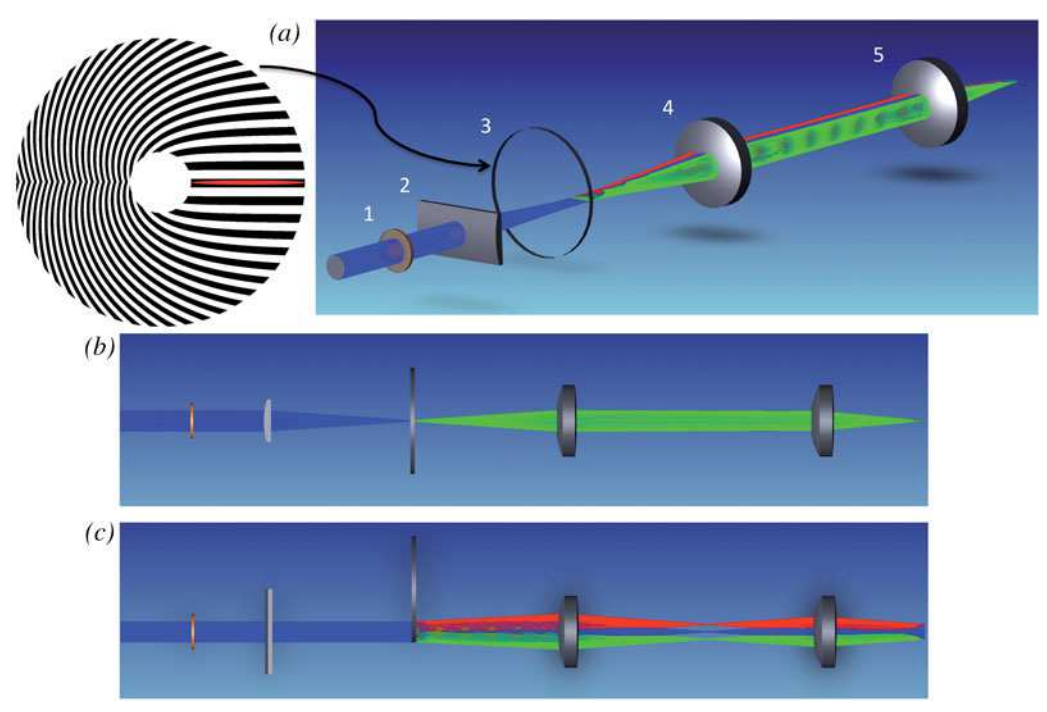


Figure 5. Depiction of multiple views of the standard SPIFI optical system. (a) is an isometric view with (1) the waveplate controlling the polarization of the beam at the entrance to the system, (2) cylindrical lens, (3) modulation mask, (4) relay lens, and (5) the objective lens. The reticle pattern to the left of (a) shows an example modulation mask with the laser focus shown in red along the radius. (b) shows a Y-Z view, and (c) shows the orthogonal X-Z view of the system. In all cases, the red, green, and blue beams represent the three diffracted orders (-1, 0, +1) considered for imaging.

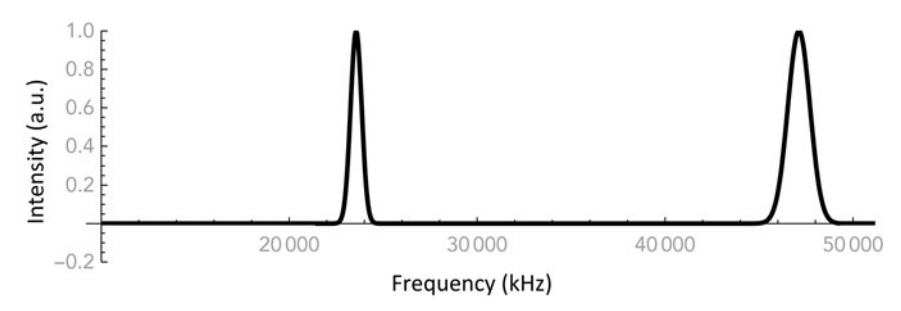


Figure 6. Modeled 1D SPIFI image showing the reconstructed first and second orders after a complete rotation of the modulation mask. In this modeled example, the first order image is centered at a carrier frequency of 24 kHz, and the second at 48 kHz.

images separated at two distinct carrier frequencies. In this case the image is of the laser excitation source and reconstructs the Gaussian intensity profile of the laser beam. The impressive utility of SPIFI is quite evident here: the first order standard resolution image is isolated at one carrier frequency (in this example it is 24kHz) and the second order enhanced resolution image is isolated at twice that carrier frequency (in this case 48 kHz). Once again, this all happens automatically with careful design of the SPIFI mask and attention to the sampling conditions. More generally, Field et al. [3] have shown that for multiphoton imaging modalities, an excitation process that scales as  $I^{\eta}$  (I being defined as the excitation intensity and  $\eta$  defined as the order of the nonlinear process) results in spatial resolution gains up to  $2\eta$  below the diffraction limit!

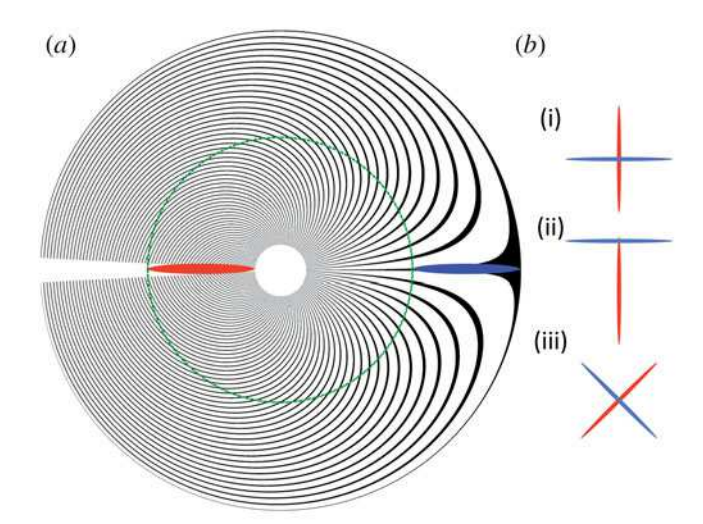


Figure 7. Simple depiction of the laser positions on the machined modulation mask. (a) is a low resolution modulation mask with the focal locations of both the horizontal (blue) and vertical (red) dimensions. (b) shows example configurations of the line foci at the sample which may be desired for different scenarios.

#### 1.2. Extension to multiple dimensions

It is possible to extend the modulation pattern projected onto the sample from a single dimension to an arbitrary number of dimensions by sending multiple beams through the microscope and individually rotating them to the desired set of angles at the sample plane. The beams can also be offset axially by adding a defocus term to one beam relative to any other. As long as the beams have a different carrier frequency, their reconstructed image will be separate after Fourier transforming the collected signal. This can be accomplished by focusing two beams onto different portions of the SPIFI mask as is shown in Figure 7.

The primary advantage of this scheme is the ability to retrieve the enhanced resolution image in both dimensions simultaneously. SPIFI provides enhanced resolution in the direction along the modulation axis of the beam, but while scanning either the object or the illumination beam during image acquisition, the resolution in the perpendicular direction is determined by the spot diameter and/or the step size between successive scans. In the microscope described below, two modulated imaging beams are made incident on the object in orthogonal orientations so that enhanced resolution is simultaneously generated in both lateral dimensions on the sample for the first time.

# 2. Microscope and machined modulation design

# 2.1. Optical components and microscope design

The laser used as the illumination source for this microscope was an all-normal dispersion (ANDI) Yb-fiber oscillator<sup>[16]</sup> which has a central wavelength of 1040 nm. The microscope (Figure 8) consists of two identical 100 mm focal length cylindrical lenses ( $L_{CA1}$ ,  $L_{CA2}$ ) (Thorlabs LJ1567L1-B) that are placed after a polarizing beam splitter (PBS) (Thorlabs PBS253) in both the reflection and transmission directions. A half wave plate (HWP) is placed before the beam splitter to control the power in both arms of the microscope. The laser is focused by these lenses to the surface of the fused silica modulation mask (MM). Both arms 1 and 2 are then re-imaged in a 4-f configuration by 75 mm focal length lenses ( $L_{1A1}$ ,  $L_{1A2}$ ) (Thorlabs LA1145-B) which are placed 2f (150 mm) from the substrate. Arm 1 has a 50 mm lens ( $L_{2A1}$ ) (Thorlabs LA1131-B) placed away from the image plane by its focal length, while Arm 2 consists of two 100 mm focal length

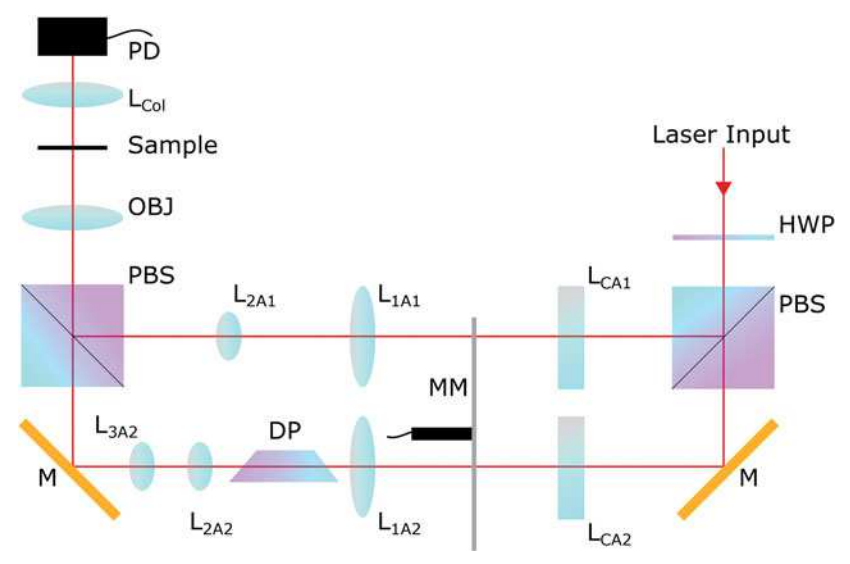


Figure 8. Layout of the multi-dimensional SPIFI microscope consisting of the two independent beam lines. The input is separated by a polarizing beam splitter, where both lines are then focused to the modulation mask by cylindrical lenses. After modulation, both beams are image relayed by their respective lenses and the objective lens to the sample plane through an additional polarizing beam splitter which makes both arms of the microscope co-linear. Arm 2 also contains a dove prism (DP) which can be rotated to an arbitrary angle, which makes this multidimensional imaging possible.

lenses (L<sub>2A2</sub>, L<sub>3A2</sub>) (Thorlabs LA1509-B). The first of which is placed 43 mm from the image plane, and the second is separated from the first by 78.8 mm. This results in an effective focal length of 35.97 mm. Arm 2 also has an uncoated N-BK7 dove prism (DP) (Edmund Optics 32-553) with a clear aperture of 15 mm. This prism is rotated to an angle of 45° with respect to the vertical direction, which rotates the modulated beam by 90°. The beams from each arm of the microscope are then recombined and made co-linear with another polarizing beam splitter (Thorlabs PBS253). The beams are imaged to the sample plane by an objective lens with a focal length of 125 mm (OBJ) (Thorlabs LA1384-B). In the current geometry with the dove prism at a 45° angle, the two beams incident on the sample form an orthogonal cross pattern (Figure 7(b,i)), with the central points of each beam overlapped. If desired, the prism in Arm 2 may be rotated to any angle to rotate the beam by the desired arbitrary amount, or one beam may be moved relative to the other (as in Figure 7(b,i-iii)). When the image is made in the transmission direction, a 75 mm focal length lens ( $L_{Col}$ ) (Thorlabs LA1145-B) is placed behind the sample and focuses the light onto a photodiode where the temporal data is collected and processed to form the final images.

By rotating the beam(s) after modulation the optical delivery system is simplified, as both beams are incident on the mask at the same height and orientation with respect to the optical table. This removes the need for any height adjustments (e.g., periscope) to make the beams colinear. The single modulation mask design also creates a system where there is no need for synchronization between the collected temporal signals of the different projected dimensions. The phase offset in the collected signal for each dimension is set by the angular difference of the two beams on the modulation mask. In the system described here, the orthogonal dimensions are offset by exactly half of a revolution/scan of the modulation mask (180°).

# 2.2. Advantages of a single machined modulation mask design

One method of extracting two dimensional images from a SPIFI system has been demonstrated by, [17] wherein two modulation masks are placed one after the other in orthogonal orientations. In this scheme the 2 D field of view is illuminated by the imaging beam and an algorithm is put in place to extract the image from the cross terms generated by the interference of the two dimensions.

For this new imaging system design, a single standard SPIFI modulation pattern was machined from a 75 mm diameter, 3 mm thick fused silica substrate. The two beams used to form the final image are made incident on the mask by two cylindrical lenses oriented with their axes of optical power perpendicular to the horizontal radius of the modulation mask. This results in the line focus created by each lens to be along the radius of the mask. The two beams are laterally offset along the radius of the modulation mask by 55 mm and each have a lateral extent of 5.3 mm. This lateral separation and beam size create a situation where the two beams each are comprised of a unique portion of the overall bandwidth of the modulation mask in addition to the beams having distinct carrier frequencies. The unique frequency composition of each beam makes it possible to simultaneously collect the modulated signal from both imaging beams without the creation of cross terms in the collected signal between the dimensions which eliminates any specialized algorithms for image reconstruction. By ensuring that there is no spatial overlap between the beams in the single mask design, it is guaranteed that the frequency spaces of the individual beams are unique. By following this simple constraint, any number of beams may be focused onto the modulation mask and imaged to the sample without risk of one beam interfering with another in terms of the temporal signal generation.

Regardless of the modulation scheme used, it is crucial to sample the collected signal at a fast enough rate to ensure that the maximum NA of the final imaging optic is exploited. Futia et al. [1] detail the necessary temporal sampling rates of the detector signal to ensure the highest possible spatial resolution in SPIFI.

By doing so, this ensures that the maximum resolution provided by the mask is obtained. As an example, for the imaging system described in this paper, the detector signal was sampled at >300 kHz, which is far above the rate required for the fundamental resolution reconstructed images centered around 25–34 kHz. These signals only required of 50–68 kHz rate to satisfy the Nyquist sampling constraints. It is also important to sample above the Nyquist frequency of the enhanced resolution signals if the intent is to fully reconstruct the enhanced resolution images. For this imaging system, the carrier frequencies of these enhanced resolution signals were 50 kHz and 68 kHz which require 100 kHz and 136 kHz sampling rates respectively.

The reason why a set of line foci are used in this microscope as opposed to a 2D wide field illumination comes down to simple photon economics. As an example, a two-photon excitation fluorescence process (TPEF) can typically require illumination intensities of  $\geq 100 \frac{GW}{cm^2}$ . For scale, this means that for a  $1\,\mu$  m spot size, a pulse with energy of  $\geq \! 100 pJ$  and a temporal duration of 100 fs is required. These parameters are attainable by use of solely an ultrafast laser oscillator. When extended to a line focus with example parameters of 300  $\mu$  m by  $1\,\mu$  m, the pulse energy required to meet the illumination intensity threshold rises to  $\sim \! \! 30\, nJ$  for a 100fs long pulse. Pulses in the tens of nanoJoule range are also attainable by ultrafast laser oscillators. There is a large step up in the required energy for illuminating a wide field with enough intensity for a TPEF process, however. When considering a field of view of 300  $\mu$  m by 300  $\mu$  m, it requires 100 fs pulses with an energy of  $\geq 9\,\mu$  J. These energies usually require an amplified ultrafast system and are thus much less accessible.

#### 2.3. Modulation mask machining and path generation

In order to machine the modulation mask for the microscope, the modulation equation is sampled with the desired parameters in a binary fashion over the area of the substrate that will be machined. Next, the resulting image is run through a morphological component analysis, which separates all of the unique sections of the modulation pattern. A shortest tour algorithm is run on each of the sections to create the path that the laser will traverse when ablating the

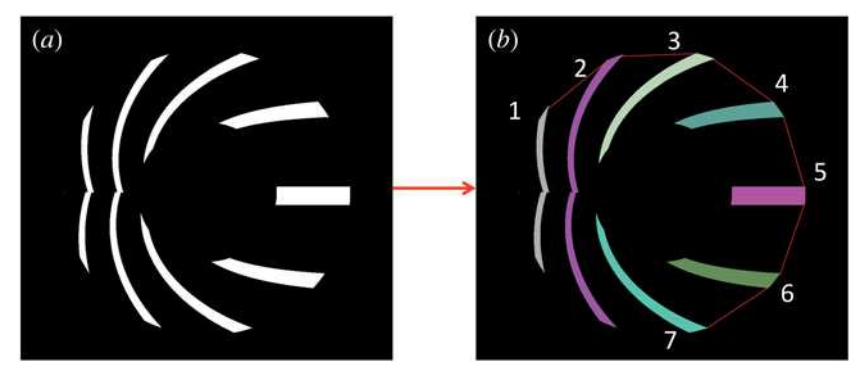


Figure 9. Depiction of a simple mask design showing the steps followed in order to machine the modulation masks. (a) Is the standard pattern generated from Equation 14. (b) Shows the results of the morphological component analysis which splits the pattern up into its unique sections. These are shown with different colors and numbers and are connected by red lines which indicate when the laser is lifted out of the substrate and is translated to the next section of the mask.

pattern, and then all of the code for each of the sections are placed one after another. Care is taken to ensure that when the machining laser has to transverse more than one diameter of the focal spot from a single point to the next that the stages lift the substrate away from the focal plane so that there is no unwanted ablation across the substrate.

Examples of this process can be seen in Figure 9. For illustration purposes, a low resolution modulation mask is generated (Figure 9(a)). The pattern is then separated into its unique sections (colors in Figure 9(b)) so the laser path can be generated for each portion individually. To travel from one section to another, the laser spot is lifted out of the substrate and traverses the lines shown in red within Figure 9(b).

Images of the transmission mask machining and the mounting bracket used to attach it to the rotation motor can be seen in Figure 10, where Figure 10(a) was an image taken while the mask was being machined, and Figure 10(b) shows the machined mask with the metal mounting bracket installed.

The modulation mask substrate was machined with  $\Delta \kappa = 10 \text{mm}^{-1}$  down to a minimum feature size of  $7\,\mu\,m$  by an amplified femtosecond laser with a central wavelength of  $1040\,nm$  and pulse duration of 185 fs. [4,18] A spot size of 16 µm FWHM was used with an average power of 137 mW (13.7  $\frac{\mu J}{\text{pulse}}$  at a repetition rate of 10 kHz, pulsewidth of  $\sim$ 200 fs) to ablate the fused silica substrate. The total fabrication time was approximately 20 h.

# 3. Experimental data

# 3.1. Signal capture and image generation

Examples of the temporal signal generated by the two arms of the microscope can be seen in Figure 11. The corresponding Fourier transforms of the two arms which highlight the lack of frequency space overlap between the beams can be seen in Figure 12. These signals were collected with no object placed at the sample plane of the microscope so that the undisturbed beam profile of both imaging arms of the microscope could be collected. This was to ensure that the separation of the two beams on the mask was enough to separate their carrier frequencies and supported bandwidths. The results of this can be seen in Figure 12.

The temporal data was captured with a data acquisition card (DAC) from National Instruments (NI-USB-6341) and a silicon photodiode from Thorlabs (DET100A Si Biased Detector). The software used was a custom-built program that reads in the triggered temporal time signal and records it to a data file while moving the translation stages in the appropriate manner to form the 2D images for each arm of the microscope. The data collection card is

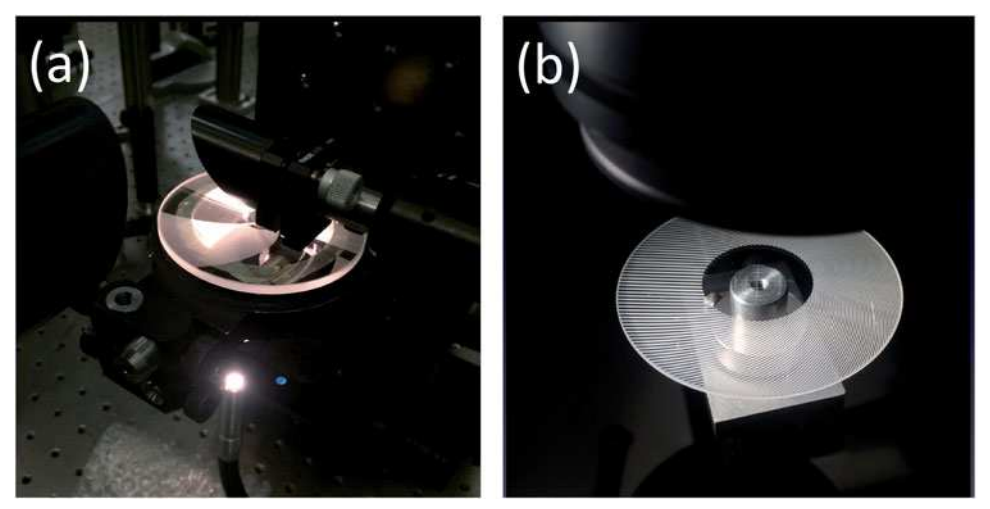


Figure 10. Images of the modulation mask machining and mounting. (a) Shows the mask while it is machined by the femtosecond laser, and (b) Shows the mask after installation of the mounting bracket that attaches to the rotation motor.

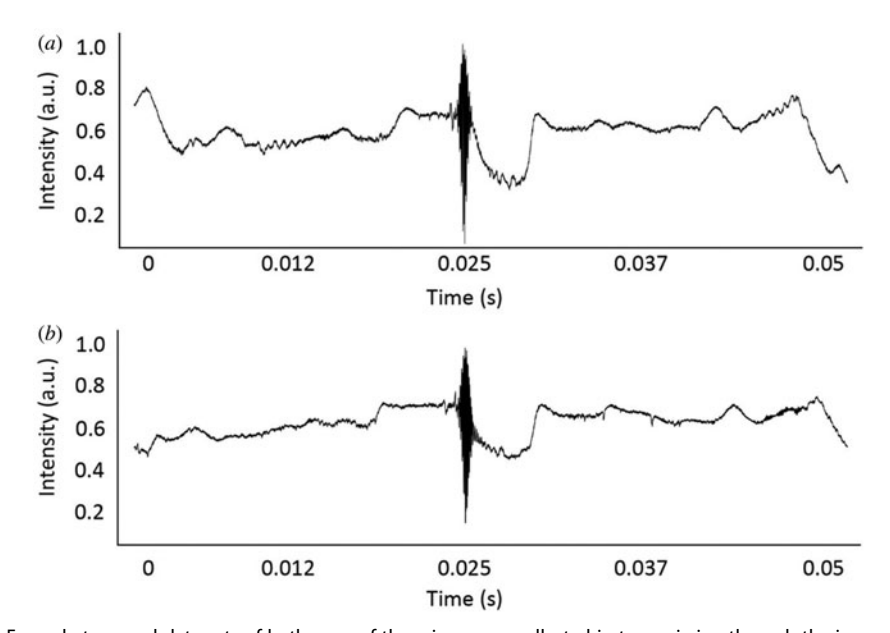


Figure 11. Example temporal data sets of both arms of the microscope collected in transmission through the image plane. (a) Is representative of the data from Arm 1 of the microscope, and (b) Is the temporal data from Arm 2.

triggered for each image by an additional photodiode and a 635 nm diode laser is incident on the surface of the modulation mask. The collected temporal signal is then processed, and Fourier transformed into a frequency-space image where the standard and enhanced resolution images can be viewed for each dimension.

# 3.2. Multi-dimensional images

Images were made with both arms of the microscope of an Air Force 1951 resolution target in order to examine the resolution of the microscope. The calculated resolution of the system is 86  $\mu$ m from Arm 1, and the resolution of Arm 2 is 63  $\mu$ m. The measured resolution is between

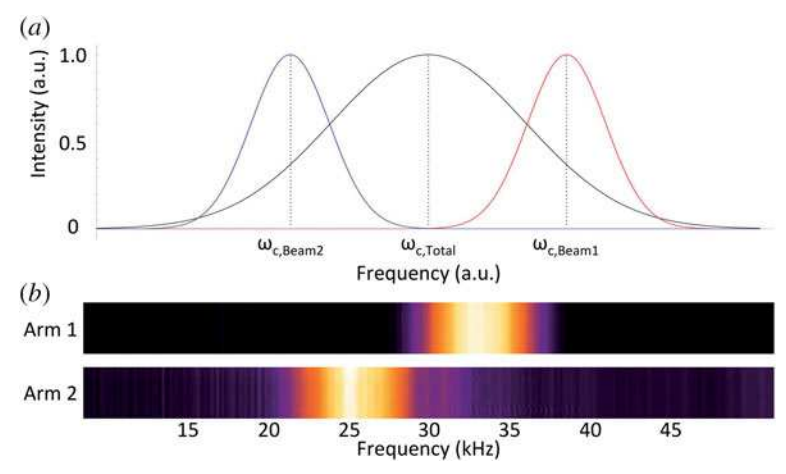


Figure 12. Examples of the two beam profile locations in frequency space. (a) Is a simple representation of the frequency content of the two imaging beams within the microscope (blue and red) relative to the overall frequency content of the modulation mask (black). (b) Shows the reconstructed images of the beam profiles of both arms of the microscope which confirm sufficient frequency space separation.

88.4 μm and 78.8 μm for Arm 1 and 70.2 μm and 62.5 μm for Arm 2 according to the groups on the resolution target. Example images of the target are shown in Figure 13(a,c). Enhanced resolution images were formed in both arms of the microscope as well and can be seen in Figure 13(b,d). The same section of the resolution target was imaged in both arms and the images were then rotated post-collection to be in the same orientation.

A complete reconstructed image example of the AF resolution target is shown in Figure 14. Figure 14(a) shows the 2 D image which highlights both reconstructed image orders, and the red line shows the location of the full 1D reconstructed image in Figure 14(b). This image demonstrates experimental verification of the results in Figure 6, with the width of the second order image being twice that of the first, in addition to the carrier frequency of the second order image (68 kHz) being twice that of the first order image (34 kHz).

Additional images were also made of some portions of a machined structure that was ablated on a microscope slide in order to further demonstrate the benefits of the enhanced resolution capabilities of this imaging technique. Figure 15(a,b) show a situation where there are features visible in the second order image which are not observable in the first order.

# 3.3. Example of potential application: Impact of multi-dimensional SPIFI for in-situ process monitoring of additively manufactured components

The novel microscope design described in this paper may have a great impact on laser based additive manufacturing (AM) technologies and other advanced manufacturing communities when it comes to the challenge of developing in-situ optical process monitoring techniques. A review by Everton et al. [19] describes the current state of the art within the field and states the many challenges it faces when attempting to image a variety of AM processes including Laser Powder Bed Fusion (LPBF) and Directed Energy Deposition (DED). Many current techniques involve high speed 2D cameras which attempt to image the dynamic processes within a small field of view (~500 μ m)<sup>[20]</sup> and generate hundreds of megabytes per second of image data. Multidimensional SPIFI allows for single element detection of multiple imaging beams without the need for a conventional camera, this allows for imaging with a decrease in the data rate that needs processing as well as imaging over large fields of view (e.g., >20 mm) with enhanced resolution as described previously. In addition, by placing the multiple imaging beams in an

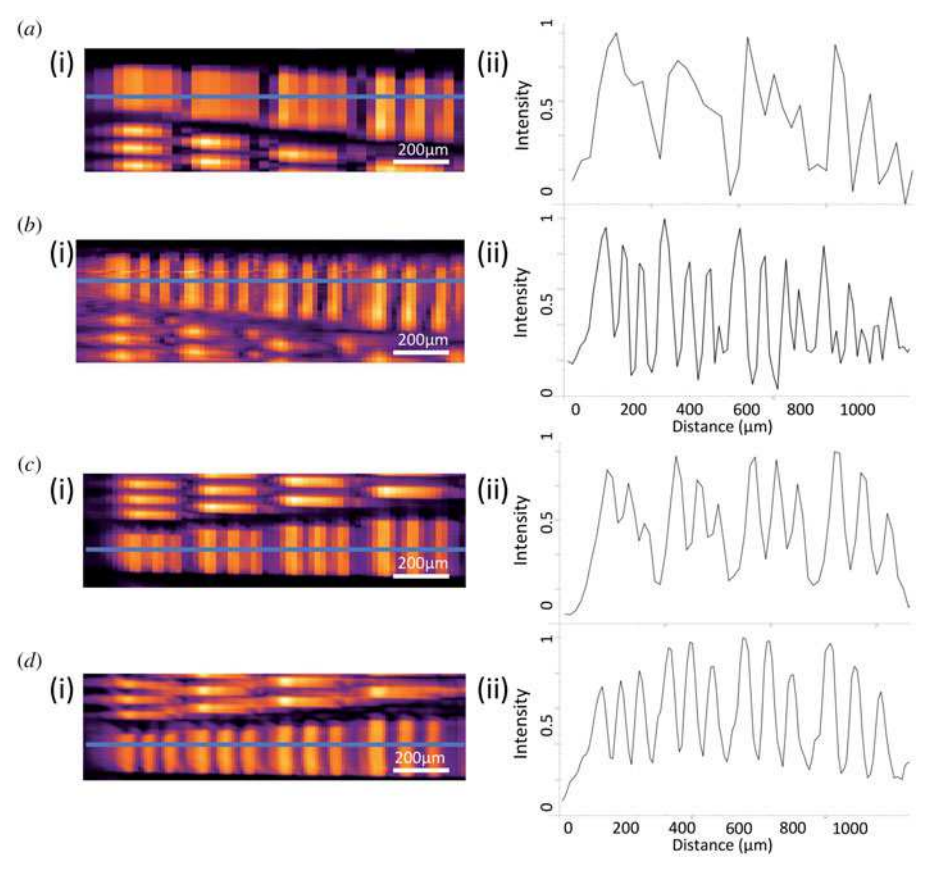


Figure 13. Images of a 1951 AF resolution test target. (a,i–ii) are the standard resolution 2 D and 1 D image of line pairs on the resolution target formed by Arm 1 of the microscope, and (b,i–ii) are the corresponding enhanced resolution images. (c,i–ii) and (d,i–ii) are the standard and enhanced resolution images from Arm 2 of the microscope.

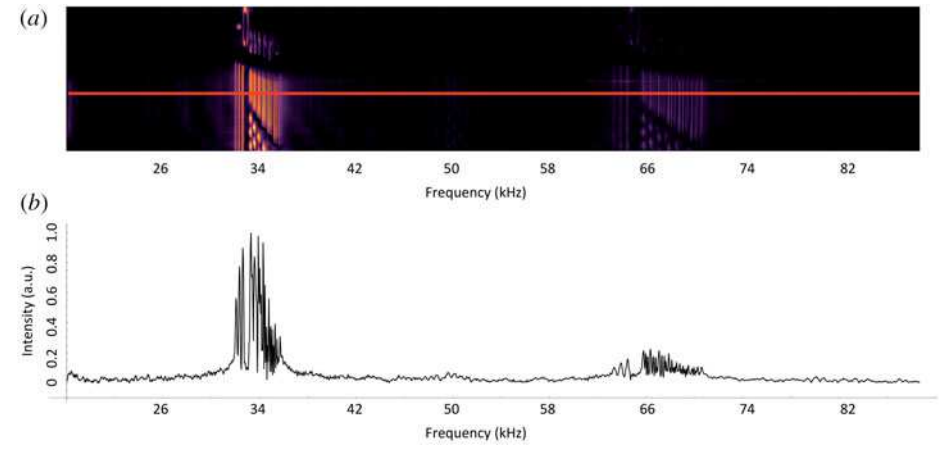


Figure 14. Example images of a portion of an 1951 AF resolution target showing both first and second order reconstructed images. (a) Is the full 2 D reconstructed image, with the red line representing the 1 D image shown in (b).

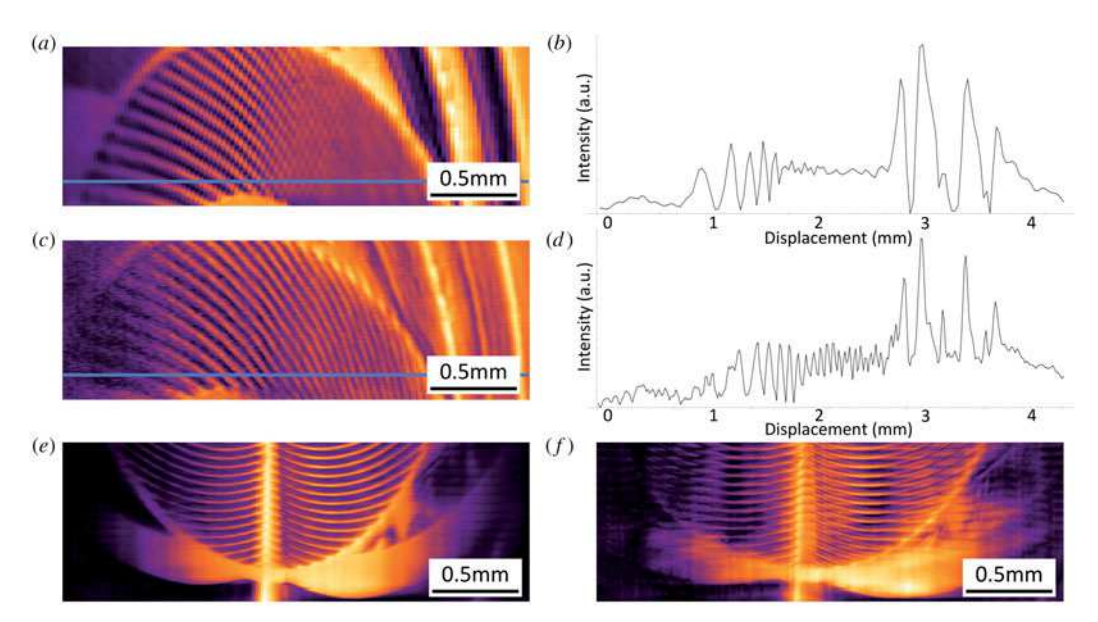


Figure 15. Images of machined structures on a glass microscope slide. (a) and (b) are the 2D and example 1D standard resolution images created by Arm 1 of the microscope, and (c) and (d) are the corresponding enhanced resolution images. (e) and (f) are the enhanced and standard resolution images formed by Arm 2 of the microscope.

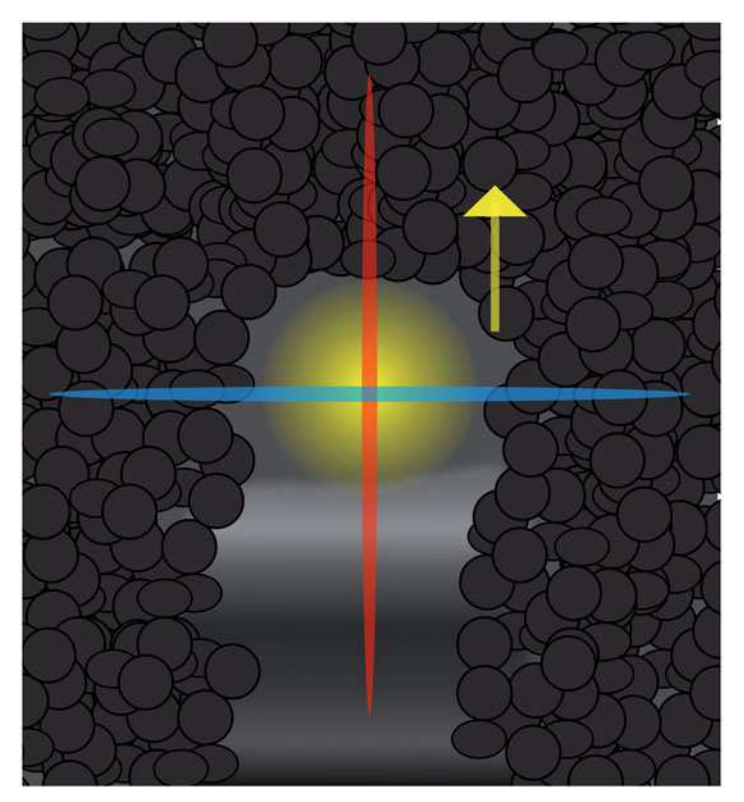


Figure 16. Depiction of imaging the melt pool in a LPBF process with the multi-dimensional SPIFI system. The central yellow spot represents the melting laser creating a melt pool on the surface of the powder bed (gray spheres), with the movement direction indicated by the yellow arrow. The red and blue crossed-beams represent the two SPIFI imaging directions.

orientation which is a variation of those shown in Figure 7(b) it is possible to simultaneously examine arbitrary dimensions along the melt pool of a dynamic AM process. A simple depiction of the proposed imaging conditions is shown in Figure 16.

The gain in data efficiency with the 2 D SPIFI system is evident through straight forward comparisons. For example, a 2 D SPIFI system with 512 pixels per cursor, when compared to a 2 D camera sensor with a 512 by 512 matrix of pixels, represents only 0.4 percent of the net pixels (compared to the 2 D camera sensor), and produces a higher resolution image. This reduction in data makes it possible to envision realistic feedback control systems that can rapidly process the high resolution image flow enabling real time correction of any flaws that are detected.

To date we have constructed a novel chamber system to test the approach detailed here. We have signals off the powder bed and can track when the fusing laser modifies the powder. We are presently designing and implementing a scanning system which when complete, will allow us to fully vet the proposed application of SPIFI and explore its potential as an optical metrology tool for advanced manufacturing in LPBF processing.

# 4. Conclusions

Multi-dimensional SPIFI images were generated and enhanced resolution was simultaneously demonstrated in two orthogonal directions on multiple samples for the first time within a single microscope system. The new technique may be expanded from two, to an arbitrary number of modulated beams provided that their carrier frequencies and supported bandwidths are all offset by the necessary amount so that signal from one dimension does not extend into another. This method is significant, as multiple illumination beams with different characteristics (e.g., polarization, wavelength, various imaging depths, etc.) can be imaged at the same time within a single platform.

By forgoing collection of an entire field of view and relying on scanning multiple modulated line foci, nonlinear imaging modalities such as second harmonic generation (SHG), third harmonic generation (THG), two photon excitation fluorescence (TPEF), etc. become more accessible, as the extremely energetic laser pulses needed to generate significant signal over the entire imaging area are not necessary.

In addition, for a dynamic process such as imaging the melt pool formation during additive manufacturing or dynamics that occur during other machining or imaging situations, it allows the simultaneous imaging of multiple axes (e.g., laterally and longitudinally along an ablated channel). The ability to visualize these processes as they occur could also allow for the implementation of a feedback control within the system to converge on the desired parameters in a more rapid manner.

#### **Funding**

Worts acknowledges support from Moog Inc. 500 Jamison Rd Plant 20, East Aurora NY 14052. J. Squier acknowledges support from the National Science Foundation (NSF) [1707287]; NeuroNex Technology Hub:Nemonic: Next generation multiphoton imaging consortium. J. Czerski acknowledges support from the Department of Defense, Office of Economic Adjustment [# ST1605-17-02]. R. Bartels gratefully acknowledges funding support from the National Institute of Health (NIH) [R21EB025389, R21MH117786]. The content is solely the responsibility of the authors and does not necessarily represent the official views of the National Institutes of Health.

#### References

[1] Futia, G.; Schlup, P.; Winters, D. G.; Bartels, R. A. Spatially-Chirped modulation imaging of absorbtion and fluorescent objects on Single-Element optical detector. *Opt. Express* **2011**, *19*, 1626. DOI: 10.1364/OE.19. 001626.



- Howard, S. S.; Straub, A.; Horton, N. G.; Kobat, D.; Xu, C. Frequency multiplexed in vivo multiphoton phosphorescence lifetime microscopy. Nat Photon. 2013, 7, 33–37. DOI: 10.1038/nphoton.2012.307.
- [3] Field, J. J.; Wernsing, K. A.; Domingue, S. R.; Allende Motz, A. M.; DeLuca, K. F.; Levi, D. H.; DeLuca, J. G.; Young, M. D.; Squier, J. A.; Bartels, R. A. Super-Resolved multiphoton microscopy with spatial Frequency-Modulated imaging. Proc. Natl. Acad. Sci. U S A. 2016, 113, 6605-6610. DOI: 10.1073/pnas. 1602811113.
- [4] Worts, N.; Young, M.; Field, J.; Bartels, R.; Jones, J.; Squier, J. Fabrication and characterization of modulation masks for multimodal spatial frequency modulated microscopy. Appl. Opt. 2018, 57, 4683. DOI: 10. 1364/AO.57.004683.
- Diebold, E. D.; Buckley, B. W.; Gossett, D. R.; Jalali, B. Digitally synthesized beat frequency multiplexing [5] for Sub-Millisecond fluorescence microscopy. Nat Photon. 2013, 7, 806-810. DOI: 10.1038/nphoton.2013.
- [6] Block, E.; Young, M. D.; Winters, D. G.; Field, J. J.; Bartels, R. A.; Squier, J. A. Simultaneous spatial frequency modulation imaging and micromachining with a femtosecond laser. Opt. Lett. 2016, 41, 265. DOI: 10.1364/OL.41.000265.
- Field, J. J.; Winters, D. G.; Bartels, R. A. Single-Pixel fluorescent imaging with temporally labeled illumination patterns. Optica 2016, 3, 971. DOI: 10.1364/OPTICA.3.000971.
- [8] Worts, N.; Field, J.; Bartels, R.; Jones, J.; Broderick, J.; Squier, J. Interferometric spatial frequency modulation imaging. Opt. Lett. 2018, 43, 5351-5354. 2018/11/01 DOI: 10.1364/OL.43.005351.
- [9] Field, J. J.; Squier, J. A.; Bartels, R. A. Fluorescent coherent diffractive imaging with accelerating light sheets. Opt. Express. 2019, 27, 13015-13030. DOI: 10.1364/OE.27.013015.
- [10] Field, J. J.; Winters, D. G.; Bartels, R. A. Plane wave analysis of coherent holographic image reconstruction by phase transfer (Chirpt). J. Opt. Soc. Am. A. 2015, 32, 2156-2168. DOI: 10.1364/JOSAA.32.002156.
- [11] Field, J. J.; Wernsing, K. A.; Squier, J. A.; Bartels, R. A. Three-Dimensional Single-Pixel imaging of incoherent light with spatiotemporally modulated illumination. J. Opt. Soc. Am. A. 2018, 35, 1438-1449. DOI: 10. 1364/JOSAA.35.001438.
- Higley, D. J.; Winters, D. G.; Futia, G. L.; Bartels, R. A. Theory of diffraction effects in spatial Frequency-Modulated imaging. J. Opt. Soc. Am. A 2012, 29, 2579. DOI: 10.1364/JOSAA.29.002579.
- [13] Driggers, R. G.; Halford, C. E.; Boreman, G. D.; Lattman, D.; Williams, K. F. Parameters of spinning FM reticles. Appl. Opt. 1991, 30, 887. DOI: 10.1364/AO.30.000887.
- Driggers, R. G.; Halford, C. E.; Boreman, G. D. Use of spatial light modulators in frequency modulation [14] reticle trackers. Opt. Eng. 1990, 29, 1398-1403. DOI: 10.1117/12.55744.
- [15] Lovell, D. J. Electro-Optical Position Indicator, s. 1961. US Patent 2,997,699.
- Chong, A.; Buckley, J.; Renninger, W.; Wise, F. All-Normal-Dispersion femtosecond fiber laser. Opt. [16] Express. 2006, 14, 10095. DOI: 10.1364/OE.14.010095.
- [17] Winters, D. G.; Bartels, R. A. Two-Dimensional Single-Pixel imaging by cascaded orthogonal line spatial modulation. Opt. Lett. 2015, 40, 2774. DOI: 10.1364/OL.40.002774.
- [18] Squier, J.; Thomas, J.; Block, E.; Durfee, C.; Backus, S. High average power Yb:CaF2 femtosecond amplifier with integrated simultaneous spatial and temporal focusing for laser material processing. Appl. Phys. A. 2014, 114, 209-214. DOI: 10.1007/s00339-013-8106-4.
- [19] Everton, S. K.; Hirsch, M.; Stravroulakis, P.; Leach, R. K.; Clare, A. T. Review of in-Situ process monitoring and in-Situ metrology for metal additive manufacturing. Mater. Des. 2016, 95, 431-445. DOI: 10.1016/j. matdes.2016.01.099.
- [20] Pavlov, M.; Doubenskaia, M.; Smurov, I. Pyrometric analysis of thermal processes in SLM technology. In Physics procedia, vol. 5; Elsevier BV: Amsterdam, Netherlands, 2010; pp. 523-531.